行政院國家科學委員會專題研究計畫成果報告

多相直驅式電動車動力系統的設計與製作(I)

Design and Manufacture of the Power System of the Multi-Phase Direct-Driven Electrical Vehicles (I)

計劃編號: NSC 90-2212-E002-218
執行日期: 90 年 8 月 1 日至 91 年 7 月 31 日
主持人：陽毅平　國立臺灣大學機械工程學系
ypyang@w3.me.ntu.edu.tw

1. 摘要
本研究計劃承接已開發完成之三相直接驅動式車輪馬達，進一步作新一代多相直接驅動車輪馬達之設計與製作，並以車輪馬達及其驅動器之動力模組產品化爲導向，分二年進行以下研發項目：
第一年
1. 多相直驅式車輪馬達的最佳化設計與製作
2. 最佳電流驅動波形之設計與驅動器製作
第二年
3. 降低馬達力矩鏈波與驅動方式的規劃與製作
4. 專用晶片 FPGA 實現驅動控制器模組製作

關鍵詞：多相直接驅動車輪馬達，最佳化設計，最佳電流波形，鏈波消減，無感測器控制。

Abstract
This research, proceeding with the formerly developed 3-phase direct-driven wheel motor, aims to the novel design and manufacture of a multi-phase direct-driven wheel motor. The product-oriented project will provide a new module of the wheel motor and its drive. The corresponding research subjects in the following two years will include:
First year:
1. Optimal design and manufacture of multi-phase direct-driven wheel motor.
2. Optimal design of the driving current waveform.
Second year:
3. Reduction of Torque ripple with motor design and driving pattern.
4. Realization of optimal controller with FPGA.

Keywords: multi-phase direct-driven wheel motor, optimal design, optimal current waveform, torque ripple reduction

2. Introduction

Traditional power systems for EVs are composed of batteries, electric motors with drives, and transmission gears to wheels. Each subsystem converts chemical, electrical or mechanical energy into different forms, thus consuming energy through the dissipation components of windage and friction. New concepts for the design of motor and their optimal driving pattern have attracted substantial attention for the improvement of overall efficiency and reliability of EVs.

Among various motor candidates, Chang [1] provided an experts' survey and concluded that induction motor drives were preferred for EV propulsion purpose, due to their low cost, high reliability, high speed, established converter and manufacturing technology, low torque ripple/noise and absence of position sensors. However, the permanent magnet brushless dc motor featured compactness, low weight and high efficiency and therefore provided an alternative for EV propulsion. Several permanent magnet motors have been developed for EVs to fulfill the special requirements, such as high power density, high efficiency, high starting torque and high cruising speed. These motors can be classified as indirect-driven [2] and direct-driven motors [3-4].

In the class of the direct-driven motors, the axial-flux motor competes the radial-flux motor with a few strengths, such as balanced motor-stator attractive forces, better heat removal configuration, no rotor back iron and adjustable air gap, etc [5]. Zhang *et al.* [6] compared among several axial-flux permanent magnet (AFPM) wheel motors for electric cars, and concluded that the interior PM ones seemed to be the best compromise in terms of power density, efficiency, compactness and capability characteristics.

The principal requirement for the dedicated wheel motor of electrical vehicles in this research is the maximum torque with acceptable ripples, resulting from inherent cogging torque, reluctance torque and harmonics of driving currents. In addition to the synchronism, the best one of the optimal waveforms for maximized torque with confined ohm loss was found and proved to be proportional to the magnetic flux variation in the air-gap between the stator and the rotor. This research explores the same optimization technique in [7], and extends the implementation to the four-, instead of, three-phase wheel motor.

3. Motor Layout and Specifications

The novel design of the disc-type axial-flux permanent magnet wheel motor presented in this paper is a prototype for electric vehicles. The explosive graph of the wheel motor is illustrated in Fig.1. The rotor disc of the hub-in motor has 16 magnets, and is sandwiched between two plates of stator, each with 24 teeth, to form a three-phase motor.

For the same stator structure, 18 magnets in the rotor form a four-phase motor. The tire is installed on the outer case rotating with the rotor.

The final shape of this wheel motor is designed to meet requested specifications of a multifunctional optimization scheme, with various constraints, such as limited space, current density of conductor, flux saturation, and driving voltage. Instead of being Y-connected, the coils are independently wired on stator poles, and are grouped into required phases. Other specifications are listed in Table 1.

Table 1. Specifications of Electric Vehicle with Wheel Motor

Objectives	Direct driven actuator, low speed and high torque
Rated values	Rated torque: 3 kg-m/500 rpm Max. torque: 6 kg-m/150 rpm Voltage: 48 VDC Speed: rated 500 rpm, max. 1000 rpm
Environments	Range: $0\,^{\circ}C \sim 40\,^{\circ}C$
Acceleration	5 seconds for 20 m/sec

4. Magnetic Circuit Model

The 3D motor structure can be simplified to a 2D configuration, and its two-side topology is cut in half for facilitating the magnetic circuit analysis. Take the three-phase motor as an example, in a section of 360 electrical degrees, the magnetic circuit of one flux loop is composed of three teeth on each side of the stator facing towards two permanent magnets embedded in the rotor.

The Kirchhoff's voltage law calculates the magnetic flux at each branch, and in turn obtained in the air gap are the flux density

$$B_g(x,s) = \mu_0 \frac{F(x,s)}{\delta(x,s)} \tag{1}$$

and torque distribution

$$T(s) = (R_o + R_i)\frac{\partial W'(s)}{\partial s}\bigg|_{I=const} \tag{2}$$

where the coenergy store is

$$W'(s) = \mu_0 (R_o - R_i) \int_0^{2\pi R} \frac{F^2(x,s)}{\delta(x,s)} dx \quad , \tag{3}$$

the overall magnetomotive force from stator windings and rotor magnets is F, the air gap length is δ, the permeability of free space is μ_0, the outer and inner radius of the stator are R_o and R_i, respectively, x represents the peripheral coordinate along the circle of the average radius $R = (R_o + R_i)/2$, and s denotes the rotor shift.

5. Design Optimization

The compromise programming method in the multifunctional optimization system tool is applied to search for the optimal values of the design variables that maximize the following performance indices:

Motor torque: $\max \; T(s)$ (4)

Torque density: $\max \; T(s)/W$ (5)

Motor efficiency: $\max \; eff = \frac{T\omega_m}{T\omega_m + P_r + P_{cl} + P_s} \cdot 100\%$ (6)

in which W is the weight of the motor, P_r denotes the ohmic loss, P_{cl} represents the core loss, and P_s illustrates the stray loss, composed of windage, friction, noise and other less dominant loss components.

The optimization design of the motor was done in the following process. First, a set of initial guess of parameters was given. Second, the values of penalty functions and their corresponding gradients were calculated under the prescribed constraints. After searching along the maximum descent direct of the gradient, the next set of design parameters was determied. The convergence and constraint conditions were examined iteratively until the design was satisfactory.

Since the coils are independently wired on stator poles, eight parallel coils are grouped into one phase for each side of the stator of the three-phase motor, and six parallel coils are grouped into one phase for each side of the stator of the four-phase motor. Although the geometric dimensions between the three-phase motor and the four-phase motor have no quite differences, further investigation on the motor performance by the finite element method becomes necessary for the final decision.

6. Finite element magnetic analysis

The finite element tool, ANSOFT, numerically calculates the magnetic field of the 3D motor configuration. Table 2 summarizes the motor performance by the magnetic analysis. The four-phase motor has a larger torque constant per phase current than the three-phase motor. Better driving performance for the four-phase motor can be expected.

Table 2. Motor performance by the magnetic analysis (square current wave)

Geometric dimensions	3-phase	4-phase
Max. current/phase	72.4 A	54.3 A
Avg. torque (kg-m)	5.2	5.9
Torq. peak (kg-m)	6.21	6.05
Torq. const. (kg-m/A)	0.072	0.109
Motor weight (kg)	10.5	10.0
Torq. density(kg-m/kg)	0.495	0.590
Max. flux density: 1.8 T	Max. power: 3000 W	
Rated voltage: 15.2 V	Rated speed: 500 rpm	

7. Optimal Driving Waveform Design

The purpose of the design of the optimal current waveform is to make the most of limited battery electricity to get the maximum torque output as well as efficiency. According to the discussion in the last section, the optimal current waveform is determined by maximizing the alignment torque of the DC brushless wheel motor in the sense of average:

The average torque is maximized under a constraint on the average ohm loss. Hence, the performance index is expressed as

$$T_{A,avg} = \frac{1}{2\pi}\int_0^{2\pi} T_A(\theta)d\theta \quad (7)$$

subject to the constraint

$$\int_0^{2\pi} I_i^2 d\theta \le \int_0^{2\pi} 6^2 d\theta, i = a,b,c,...,h. \quad (8)$$

Both theoretical and numerical analyses are made for the optimal current waveform with the following assumptions. First, the motor is operated under the rated speed so that the back-emf induced in each phase of the motor must not exceed the driving voltage. Second, the limitation of current and power loss of the conductor is released, which was prescribed by the maximum allowable current density of the conductor due to its cross section.

In this stage, the optimal current waveforms are obtained through a 2D magnetic circuit model as well as a 3D finite element model. The former is generated by the optimizer "constr" in MATLAB for a single cost function, which is to maximize the average torque over an electric period, subject to the constraint.

It is well known that the torque constant of a dc motor is defined as the ratio of the produced torque and the corresponding phase current, and is the same as the electric constant as the proportional coefficient of the back emf and the motor's rotational velocity. The back emf waveform can thus be obtained by calculating the torque constant of the motor via the finite element tool ANSOFT with a 3D motor model. Table 3 presents the motor performances from the numerical analysis.

Table 2: Motor performance driven by various current waveforms (6 rms amp)

waveform / performance	square	2D optimal	3D optimal
Average torque (kg-m)	7.45	7.06	8.03
Maximum torque (kg-m)	7.67	7.98	8.48
Torque ripple (%)	3.23	13.09	5.66

8. Drive and Control Realization

Traditional PWM inverters offer the ability to change both the magnitude and frequency of the current inputs by the use of fixed DC voltage batteries on the electrical vehicles. Four H-bridge inverters are used for the drive of the four-phase wheel motor, each driving an independent winding phase. The directly driven electrical vehicles do not have mechanical gears for the speed transition, though the electronic gear is promising alternative. The wheel motor is now installed inside the back wheel of a motorcycle, driven by four 48V batteries, each with capacity of 26 ampere-hours. The low speed or accelerating operation usually consumes larger current with lower voltage, while the high speed or cruising operation needs higher voltage but less current. Shifting the motor windings between series and parallel connections can fulfill these driving conditions. The phase current flows into the windings of the left-half stator and through the windings of the right-half stator in the series connection structure, while in the parallel connection structure the phase current flows simultaneous through both sides of the stator. The electric gear shifting circuit includes three latching relays. Closing R2 with R1 and R3 open yields the series winding connection for low speed ranges; closing relays R1 and R3 with R2 open shifts to the parallel winding connection for high speed ranges. To avoid corruption of the power electronics due to short circuit by wrong switching of relays, the dead time control is implemented with an 8051 processor.

References

[1] L. Chang, "Comparison of AC Drives for Electric Vehicles – A Report on Experts' Opinion Survey," *IEEE AES Systems Magazine*, pp. 7-10, Aug. 1994.

[2] C.C. Chan, K.T. Chau, J.Z. Jiang, W. Xia, M. Zhu and R. Zhang, "Novel Permanent Magnet Motor Drives for Electric Vehicles," *Int. Trans. on Indus. Electro.*, Vol. 43, No. 2, pp.331-338, 1996.

[3] M. Terashima, T. Ashikaga, T. Mizuno, K. Natori, N. Fujiwara and M. Yada, "Novel Motors and Controllers for High-Performance Electric Vehicle with Four in-Wheel Motors," *IEEE Int. Trans. on Indus. Electro*, Vol. 44, No. 1, pp.28-37, Feb. 1997.

[4] F. Caricchi, F. Crescimibini, O. Honorati, A. Di Napoli and E. Santini, "Compact Wheel Direct Drive for EVs," *IEEE Industry Applications Magazine*, Vol. 26, No. 6, pp.29-32, 1996.

[5] D.C. Hanselman, *Brushless Permanent-Magnet Motor Design*, McGraw-Hill, New York, 1994.

[6] Z. Zhang, F. Profumo and A. Tenconi, "Axial Flux Machine for Electric Vehicles," *Elec. Machines and Power Systems*, Vol. 24, pp.883-896, 1996.

[7] Y.-P. Yang, Y.-P. Luh, and C.-M. Lee, "A Novel Design of Optimal Current Waveform for an Electric Vehicle Wheel Motor," *Electric Power Components and Systems*, Vol. 30, No. 7, July 2002, pp.705-721.

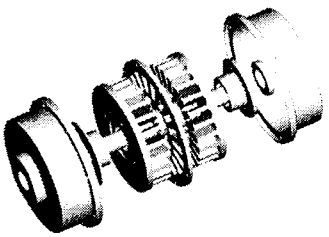

Fig. 1. The axial-flux disc-type wheel motor.

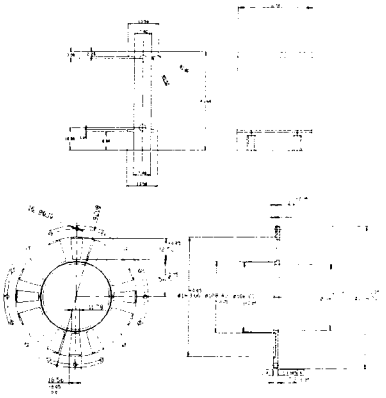

Fig. 2. Detailed geometrical features of stator tooth and rotor

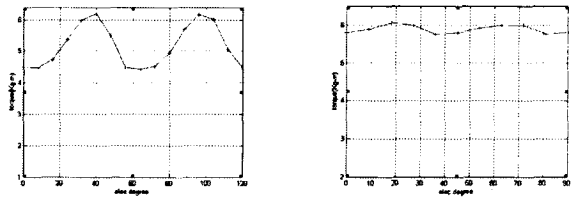

(a) (b)

Fig. 3. 3-phase (a) and 4-pahse (b) torque patterns with respect to rotor shift

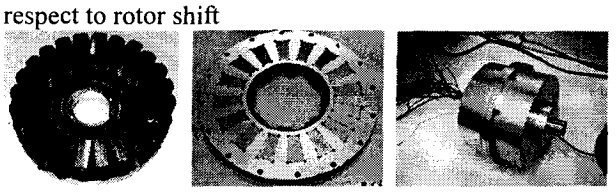

(a) (b) (c)

Fig. 4. Stator, rotor and motor assembly

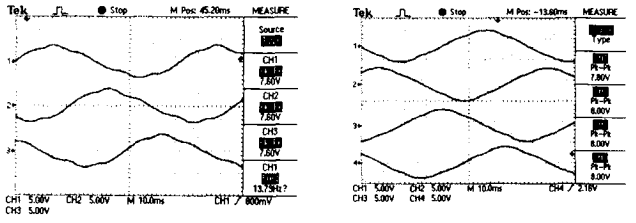

(a) (b)

Fig. 5. Back electromotive forces of the disc wheel motor

(a) 3-phase (b) 4-phase

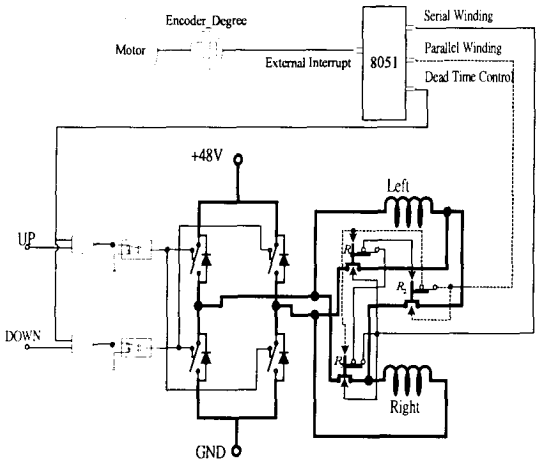

Fig. 6. Electric gear shifting circuit

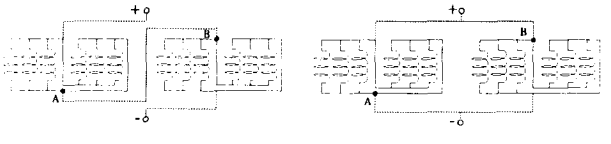

(a) Series (b) parallel

Fig. 7. Series and parallel windings

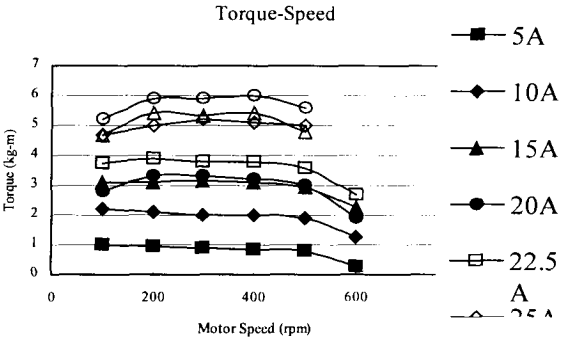

Fig. 8. Torque versus speed curves with current patterns of back emf from experiments, series winding

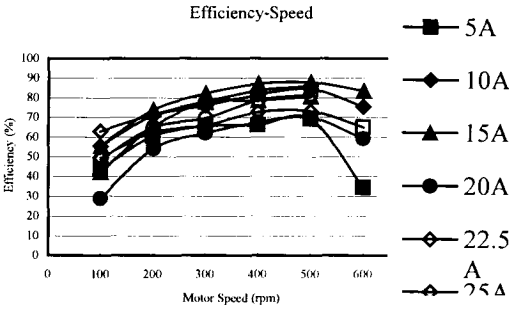

Fig. 9. Efficiency versus speed curves with current patterns of back emf from experiments, series windings.

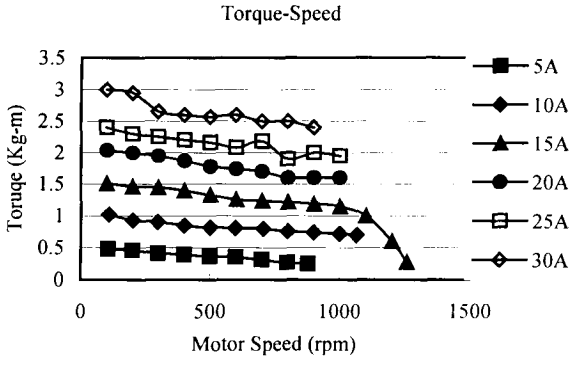

Fig. 10. Torque versus speed curves with current patterns of back emf from experiments, parallel winding

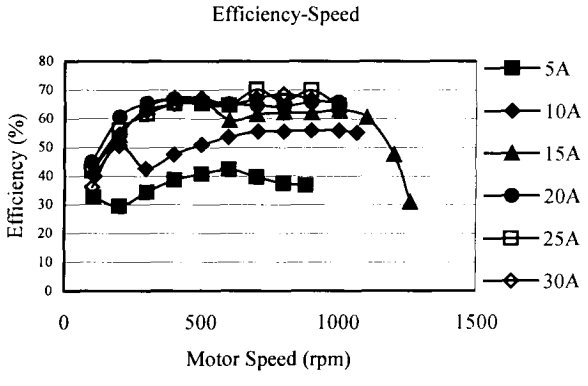

Fig. 11. Efficiency versus speed curves with current patterns of back emf from experiments, parallel winding